ORIGINAL ARTICLE

Open Access

An integrated, non-destructive method for evaluating core quality from R/V *Legend*'s giant piston coring system (LGD-GPC)

Pai-Sen Yu[1*] and Ting-Ting Chen[1]

Abstract

Despite technological advances, some core disturbances due to piston coring process still occur and can be extremely difficult to identify characteristics of sedimentary structures during qualitative visual core description and core lithologies. Few quantitative methods have offered plausible ways to define the exact magnitude of the distorted sedimentary structures in imperfect sedimentary records in the context of overly limited sedimentary records. In this study, an investigation was conducted on the Kaoping slope offshore southwestern Taiwan, a region known for its high sedimentation rate (> 0.9 g/cm^2/year), using both the LGD-GPC (giant piston corer) and giant gravity corer techniques. To examine how GPC procedures have shaped the retrieval of sedimentary sequences and affected core quality, we apply well-developed, non-destructive analyses, including physical property measurements, visible color reflectance and digital core images with quantitative curvature index (CI), to recovered sediments. Cores at 22°23'N, 120°13'E were as the basis for non-destructive measurement comparison. Evidence from digital core imaging and the CI calculation further supports the mechanism of piston suction. We suggest that shear deformation of sediment against the core barrel would be the prominent factor that govern the observed core disturbances in LGD-GPC cores. Meanwhile, excessive pulling forcing from a modified TORI piston and a slowly lift speed during LGD-GPC coring process may further aggravate core disturbances at the revisited site. The sedimentary length of core LGD-T43-B-PC is overestimated by more than 200%. We further demonstrate that an integration of the CI and color reflectance is an effective way to evaluate the transformation and distorted sedimentary sequences.

Keywords R/V *Legend*, Core disturbances, Giant piston coring, Non-destructive analyses, Curvature index, Visible color reflectance

1 Introduction

Within the regular effects of climatic forcing (e.g., Asian monsoon evolution, and typhoons) and tectonic origin (e.g., seismicity, and subaquatic landslides) in the western Pacific and East Asian continent, Taiwan is an ideal location that provides excellent material to investigate significant scientific topics across different timescales. By participating in the International Marine Past Global Change Study (IMAGES) program, Taiwanese scientists have successfully used the great capabilities of long coring systems in the last two decades, such as that on the French Research Vessel *Marion Dufresne*, to collect long cores (> 40 m) in western Pacific (e.g., IMAGES III/MD106-IPHIS cruise, WEPAMA cruise, PECTEN cruise; Chen et al. 1998; Bassinot et al. 2002; Beaufort et al. 2005). These high-quality long cores have been used in paleoceanographic reconstructions, with particular focus on tropical climate mechanisms and their teleconnections with high-latitude climates (e.g., WEPAMA/PECTEN cruises; Bassinot et al. 2002; Beaufort et al. 2005). These significant findings of late Quaternary

*Correspondence:
Pai-Sen Yu
menardii@mail2000.com.tw
[1] Taiwan Ocean Research Institute, National Applied Research Laboratories, Kaohsiung 852, Taiwan

low-latitude Pacific paleoceanography have advanced our understanding of how tropical oceans have been coupled with or isolated from the Northern Hemisphere high-latitude climate and how the tropics have played a role in modulating global climate (e.g., Chen et al. 2010; Yu et al. 2017). These findings have also provided scientific background for predicting natural/anthropogenic changes in future climates (e.g., UN Climate Change Conference, IPCC AR6; IPCC 2021).

However, little is known about the past extreme events and likely characteristics around Taiwan that were caused by earthquakes, typhoons, and climate forcings. Knowing the history of past extreme events may be critical to our understanding of their evolution and possible driving forces in comparison to natural climate mechanisms. In 2018, the Taiwan-French international team further investigated the issue of past extreme events during the R/V *Marion Dufresne* Extreme events Archived in marine GEological Records off Taiwan (EAGER) cruise. In addition, this successful EAGER cruise also reached key milestones for clean energy exploration. The trapping of frozen methane hydrate, also known as "flammable ice", in the core catcher of the Calypso corer was witnessed during the cruise. The first hand-sized hydrate was discovered in the vicinity of the South Yuan-an East Ridge. Such direct and conclusive evidence further confirms that offshore SW Taiwan has a high potential for recoverable gas hydrates (e.g., Huang et al. 2021).

For marine geological and geophysical investigations around Taiwan, the development of high-quality long coring on research vessels is necessary. In 2017, the 2800-ton R/V *Legend* operated by the Taiwan Ocean Research Institute (TORI) was equipped with a CALYPSO coring system [hereafter LGD giant piston corer (LGD-GPC)] with 8500 m length Kevlar wire and deep-sea winch system, which is similar to the R/V *Marion Dufresne* coring device. However, it is unknown whether the deployment of the free-fall LGD-GPC system affects the quality of marine sediments. The LGD-T32 and LGD-T43 cruises of the R/V *Legend* were designed to test the capability of the LGD-GPC system offshore SW Taiwan. An investigation was conducted on the Kaoping slope,

a region known for its high sedimentation rate (> 0.9 g/cm^2/year; Huh et al., 2009), using both the LGD-GPC and giant gravity corer techniques (Table 1, Fig. 1). Moreover, the characteristics of sedimentary structures are directly determined by qualitative visual core description and core lithologies. Few quantitative methods have offered plausible ways to define the exact magnitude of the distorted sedimentary structures in imperfect sedimentary records in the context of overly limited sedimentary records (Skinner and McCave, 2003; Jutzeler et al., 2014; Tommasi et al., 2019). The novel, non-destructive technique not only provide the basis for stratigraphic correlations but also give a better opportunity to understand sedimentary structures and examine the quality of the recovered sedimentary cores.

In this study, we analyze and combine non-destructive data (e.g., physical properties and visible color reflectance) in conjunction with digital core images. Cores at 22° 23' N, 120° 13' E were as the basis for non-destructive measurement comparison. This study mainly focused on (1) documenting high-resolution, non-destructive analyses on LGD-GPC and giant gravity cores from offshore SW Taiwan; (2) investigating the quality of core materials and core disturbances via non-destructive core measurements and the quantitative curvature index (CI) method; and (3) exploring stratigraphic correlations and assessing possible mechanisms, as supported by the integrated data.

2 Materials and methods

Three piston cores from the LGD-T32/LGD-T43 cruises and one gravity core, LGD-T32-C-GC, were retrieved from the same site in the Kaoping slope offshore SW Taiwan (Table 1, Fig. 1). Basic core analyses with non-destructive measurements on these marine sediment cores were mainly taken at the Marine Core Repository and Laboratory (MCRL), TORI. The lithologies of the sediment recovered during the R/V *Legend* cruises were determined using visual core descriptions. Integration of data from a multi-sensor core logger (MSCL), digital core photography, X-ray

Table 1 Giant piston/gravity cores are collected during LGD-T32 and LGD-T43 cruises

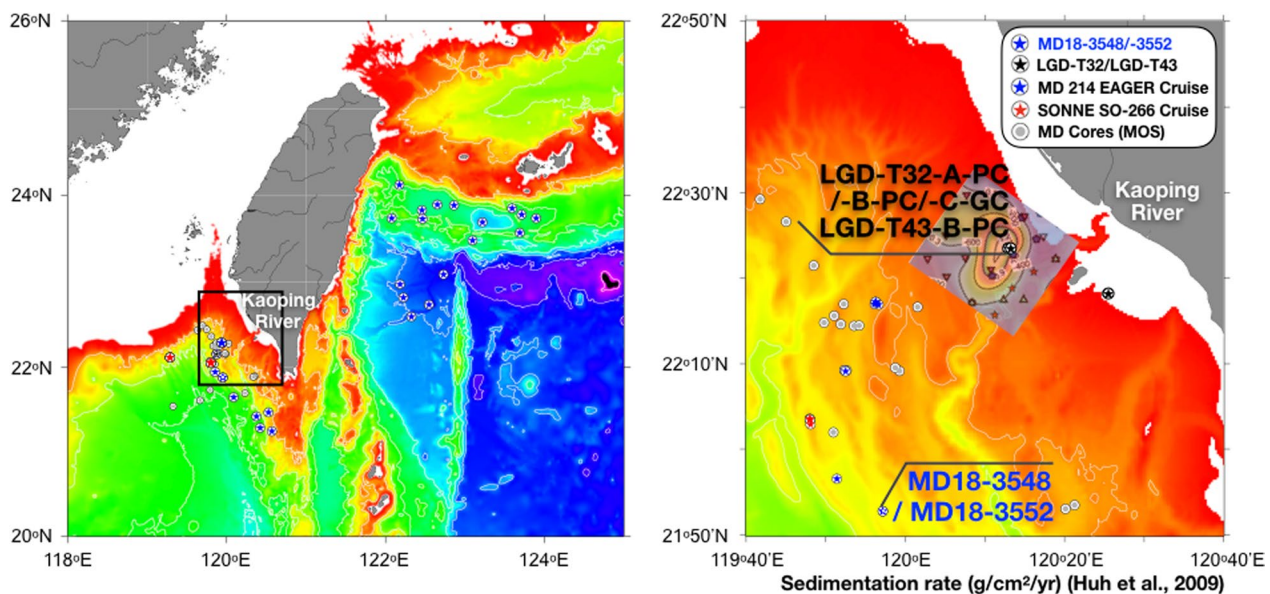| Core ID	Longitude (E)	Latitude (N)	Water depth (m)	Sediment length (cm)	Core recovery (%)
LGD-T32-A-PC	120°13.010′	22°23.267′	309	210	26
LGD-T32-B-PC	120°13.035′	22°23.283′	308	219	27
LGD-T32-C-GC	120°13.345′	22°23.288′	309	328	41
LGD-T43-B-PC	120°12.531′	22°23.493′	355	683	85

PC piston core, *GC* gravity core

Fig. 1 Locations of LGD giant piston cores (LGD-T32-A-PC/-B-PC, LGD-T43-B-PC) and LGD giant gravity core (LGD-T32-C-GC) used in this study

radiography, sedimentology and visual color reflectance spectrophotometry provided complementary information.

2.1 Non-destructive analyses

Non-destructive analyses, including analyses of physical properties, digital core images, and visual color reflectance, were performed on core material recovered during the R/V *Legend* cruises from 2020 to 2021. These analyses provide new information for the correlation of cores from almost the same sites (22° 23.5' N; 120° 12.5' E). The Geotek® MSCL with the "MST (multisensor track)" container installed in the MCRL measures the physical properties of sediment cores. The measured properties are the P-wave travel time, core diameter, temperature, gamma ray attenuation (GRA), low field susceptibility, and electrical resistivity. Using the MST, the whole cores were simultaneously logged continuously from top to bottom at 0.5-cm intervals for all marine sediment cores. Several bulk property parameters, including the P-wave velocity, gamma density, impedance, fractional porosity, magnetic susceptibility (MS), and electrical resistivity, were further generated. In addition, the derived fractional porosity is a function of the gamma density, which was calculated depending on gamma density, mineral grain density (2.650 g/cc) and water/air density (1.026 g/cc). The fractional porosity thus is directly proportional to gamma density. Those smoothly fluctuations in MS and electrical resistivity are due to non-contact sensors with 4-cm coverage, whereas other physical properties

are directly logged by point-to-point through contact sensors with scanning resolution of 5 mm. Besides, high-resolution digital core images and X-ray radiography were produced by scanning the archive half sections with a core imaging system (SmartCIS 1600SE) and a cabinet X-ray system (MINISHOT/M160NH), respectively.

Moreover, to evaluate the magnitude of the oversampling effect and the variability in core quality, a quantitative method of curvature calculation was used in this study. We followed the standards used on the R/V *Marion Dufresne* cores (Patrice et al. 2012). The quantitative indicator of CI represents a curved sedimentary layer deviation from a plane, which is calculated by a 1/height deviation from a plane (H). The curvature calculation with a CI value > 10 indicates slightly distorted sedimentary structures to horizontal structures, and a CI value in between 4 and 10 indicates moderately distorted sedimentary structures. A CI < 4 (i.e., H > 0.25 cm) means strongly distorted sedimentary structures.

2.2 Visible color reflectance analysis

Whereas the MSCL was logged through the whole-round core sections, visible color reflectance from the archive halves of the sediment cores was measured using Minolta spectrophotometer CM-700d with a narrow aperture diameter of 3 mm. Split cores covered with plastic wrap were measured at 1-cm intervals along the central line of the cores, providing

high-resolution color variations at visible wavelengths. Each measurement was recorded in 10 nm-wide spectral bands from 360 to 740 nm. Lightness (L*), a* and b* were also recorded. Moreover, wavelengths of 400–700 nm were selected for VARIMAX-rotated principal component analysis (VPCA) based on calculations of first-order derivatives. We applied a VPCA to extract the fewest statistically independent end members for modeling the maximum information preserved in the visible core reflectance data. To identify the possible mineral composition in downcore sediments, we compared downcore factor loading to color spectra of the known mineral standards database from Kent State University and the U.S. Geological Survey (USGS) Spectral Library. All color reflectance data were followed and processed according to the standard procedure from Pan et al. (2014, 2015).

2.3 Chronology

To establish a reliable chronology for all cores, accelerator mass spectrometric (AMS) radiocarbon-dated planktic foraminifer samples from the core top and core catcher was developed. Samples were processed for AMS ^{14}C dating using the same standard procedures for foraminifer identification (Imbrie and Kipp 1971). The taxonomy of planktic foraminifers follows the schemes in Parker (1962), Bé (1967), and Kipp (1976). More than 200 individuals of mixed *Globigerinoides ruber* and *Globigerinoides sacculifer* specimens with a > 150 μm size fraction (> 10 mg in weight if possible) were picked and then sent to Beta Analytic Laboratory, USA, for AMS ^{14}C dating. These raw ^{14}C conventional dates were calibrated by CALIB 8.2 software with the Marine 20 curve (Stuiver et al., 2005), and an additional regional reservoir correction was considered (ΔR value of -72 ± 39 years) and then converted to the calibration year (Stuiver and Reimer 1993). The ^{14}C conventional dates, AMS ^{14}C dates, and sedimentation rate are listed in Table 2.

3 Results

3.1 Core description

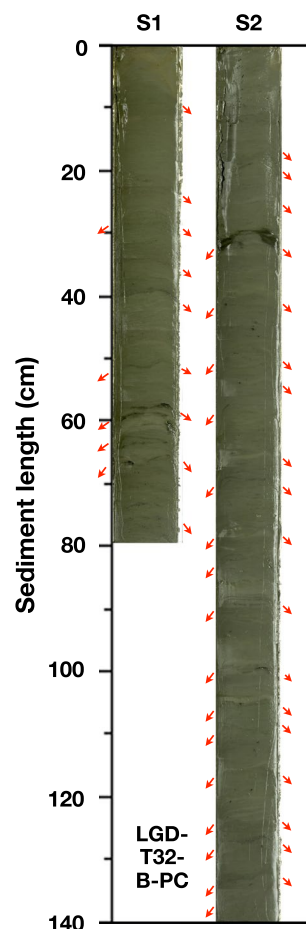In total, we recovered 210 cm and 219 cm of GPC LGD-T32-A-PC and LGD-T32-B-PC, respectively,

Fig. 2 Digital images of core LGD-T32-B-PC reveals clear features after adjusting the exposure and contrast. Vertical flowage of sediment along the core liner is significant (Red arrow)

with only 26–27% recovery for the 8 m-long core barrel. The giant gravity corer was deployed for only one core, resulting in 328-cm thick of sediment (41% core recovery for LGD-T32-C-GC). This recovery indicates that the sediment collected from the giant gravity corer required more penetration than that collected from the LGD-GPC. Unexpectedly, the giant gravity-type corer obtained a longer sedimentary sequence than the LGD-GPC. Different magnitudes of distorted sedimentary

Table 2 Radiocarbon ages used in core LGD-T32-A-PC and LGD-T43-B-PC chronology

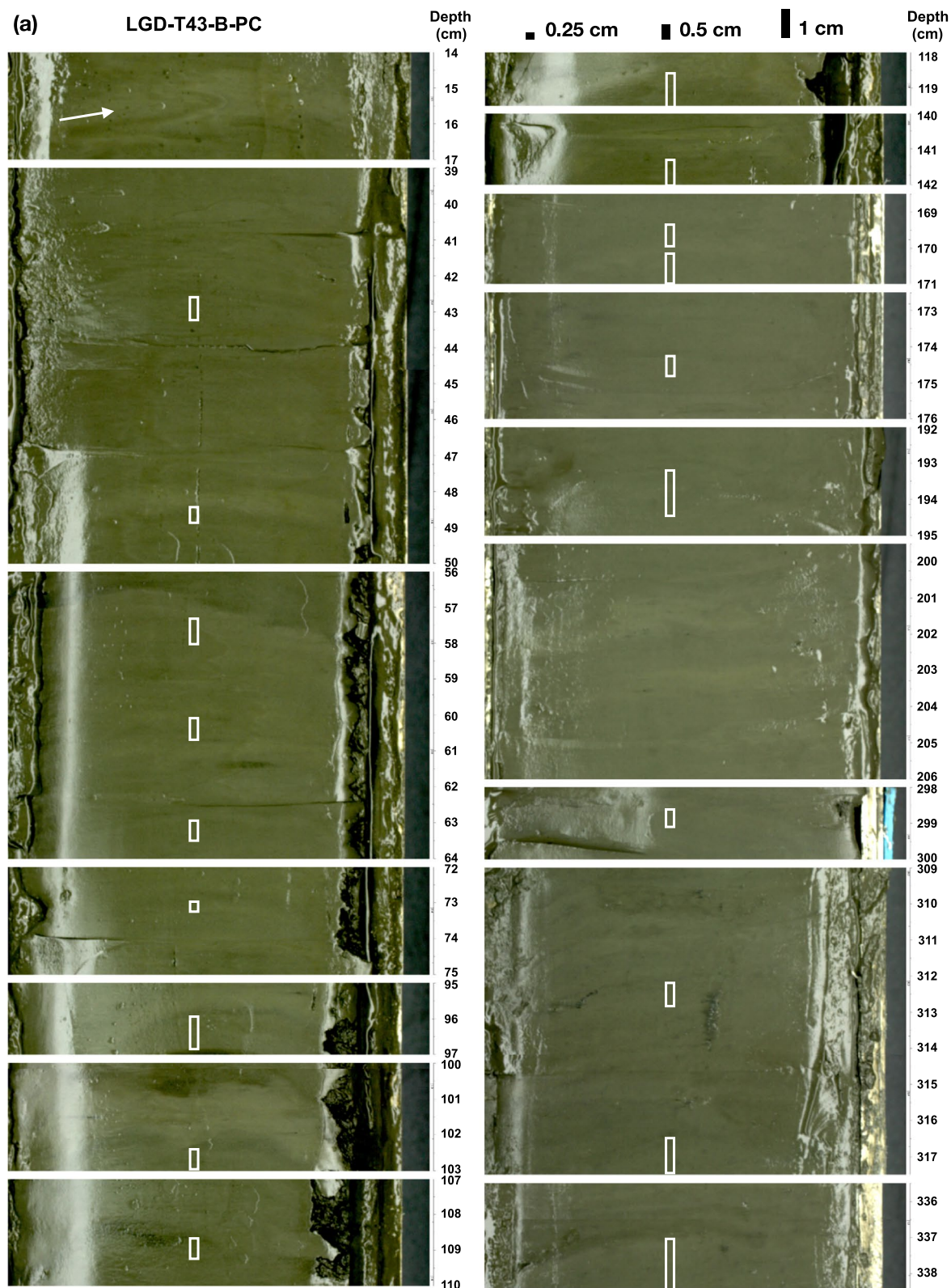| Core ID	Depth (cm)	Planktic foraminiferal species	AMS ^{14}C age (yr, BP)	Error	Calendar age (yr, BP)	Sedimentation rate (cm/yr)	Lab no
LGD-T32-A-PC	1.5	*G. ruber + G. sacculifer*	− 440	30	Modern	0.2	Beta-592654
	208.5	*G. ruber + G. sacculifer*	1440	30	893 ± 164		Beta-592655
LGD-T43-B-PC	0.5	*G. ruber + G. sacculifer*	− 740	30	Modern	0.5	Beta-591626
	683	*G. ruber + G. sacculifer*	1840	30	1316 ± 161		Beta-591627

Fig. 3 **a** Digital images of core LGD-T43-B-PC after adjusting the exposure and contrast. The CI values were calculated from heights of curvatures by selecting the significant core disturbances (White rectangle). Liquefaction can be distinguished at the top part of the core (depth of 15–16 cm; white arrow). Histograms of **b** heights of the curvatures and **c** CI values are shown respectively
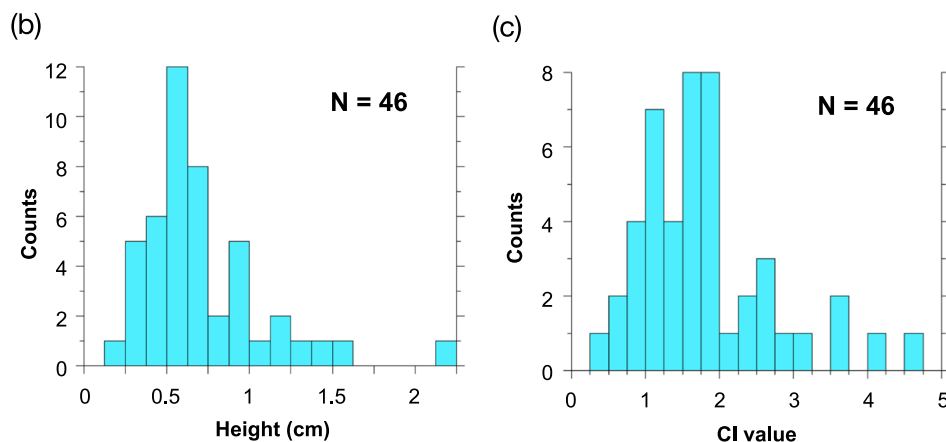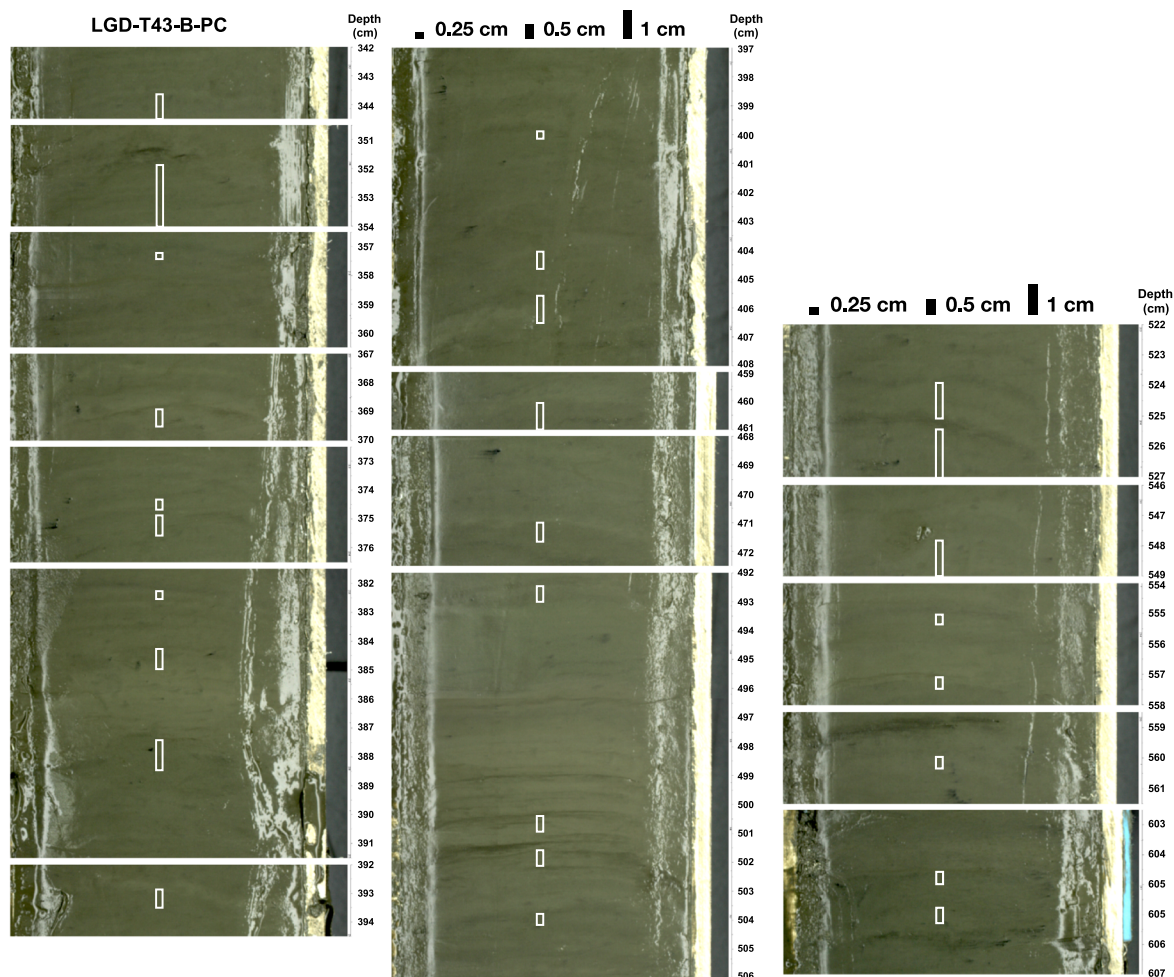
Fig. 3 continued

structures can be easily recognized in most sections after adjusting the exposure and contrast in digital surface images (Fig. 2, 3a). Most notably, nearly vertical flowage of sediment occurs along the core liner and toward the lower portion of the cores (the bottom sides) in core LGD-T32-B-PC (Fig. 2). In addition, Site LGD-T43-B-PC is at 22° 23.5' N, 120° 12.5' E and 355 m below sea level (Table 1), and it is located on the

northwestern side of the LGD-T32 sites. A total of 683 cm of core was recovered (85% core recovery) using the LGD-GPC with a modified TORI piston instead of the original piston. No hiatus or erosion of a deposited layer (or unconformity) can be found in the sedimentary sequence. The sediment is composed of homogeneous grayish silty clay to olive gray clay and several thin layers with coarse sand (Additional file 1: Fig. S1). The source of the sediments appears to be a mixture of terrestrial input with metamorphic matter that was carried by the Kaoping River. In core LGD-T43-B-PC, liquefaction (e.g., a depth of 15–16 cm) and distorted structures (e.g., depths of 100–102 cm, 200–206 cm) can also occasionally occur (Fig. 3a). It worth noting that heights of the curvatures and CI values are mainly concentrated on 0.5–1.5 cm and CI values of 1–2, respectively (Fig. 3b, c; Additional file 1: Table S1). The bent sedimentary features are more frequent and more intense in LGD-T43-B-PC (Fig. 3; Additional file 1: Fig. S2). The distorted sedimentary features with very low CI values (most close to 1) obviously appear at depths of 118–120 cm, 192–195 cm, 336–338 cm, 352–354 cm, 525–527 and 548–549 cm. The imprints of disturbance in sedimentary layers would be caused by artifact structures and would not be a response to nature sedimentary structures.

3.2 Non-destructive measurements

Though distorted sedimentary structures are broadly distributed among all the giant cores, physical property measurements along the cores were generated on whole round sections using MSCL. We regard the analyzed data of all cores to indicate a relatively less variability, but major signatures from the non-destructive analyses would be fully preserved. The non-destructive measurements of giant cores from the LGD-T32 cruise all fluctuate and have similar variations throughout the recovered succession, but those sequences have significant differences in amplitude (Fig. 4a–c). Most notably, the trend in the GRA bulk density is highly coherent with that in the acoustic impedance, but these two records mirror changes in porosity. The GRA bulk density shows an average of 1.780 g/cm^3 and ranges from 1.557 to 1.950 g/cm^3. The density exhibits a gradual increasing trend with depth. The fractional porosity range is between 0.46 wt% and 0.69 wt% (average of 0.56 wt%), indicating that the water content in the sediment is relatively low. The decreasing trend in fractional porosity may be due to lithological variations, dewatering in the pore spaces of core sediments, or a negative correlation itself between GRA bulk density and fractional porosity. P-wave

velocity measurements are performed on the portion with coarser sediments and velocity values of > 1520 m/s and fluctuate between 1470 and 1630 m/s. Most MS values are constantly stable, with values ranging between 5 SI×10^{-5} and 17 SI×10^{-5}. The average MS is 14 SI×10^{-5}, and two peaks appear in the upper and lower portions of the cores. In addition, the observations of most physical properties between those two cruises are very similar, except for the MS data (Fig. 4d). In core LGD-T43-B-PC, a clear long-term shift in MS values occurs from ~18 SI×10^{-5} to 13 SI×10^{-5}. We also found that the fluctuation in the GRA bulk density in LGD-T43-B-PC is much smoother and 0.074–0.107 g/cm^3 smaller than those of LGD-T32-A-PC and LGD-T32-B-PC (Fig. 4a, b, d). Such differences can be observed in downcore variations in the porosity and GRA bulk density. In summary, these physical properties correlate well with the interbeded clay and silty clay found in the sediments.
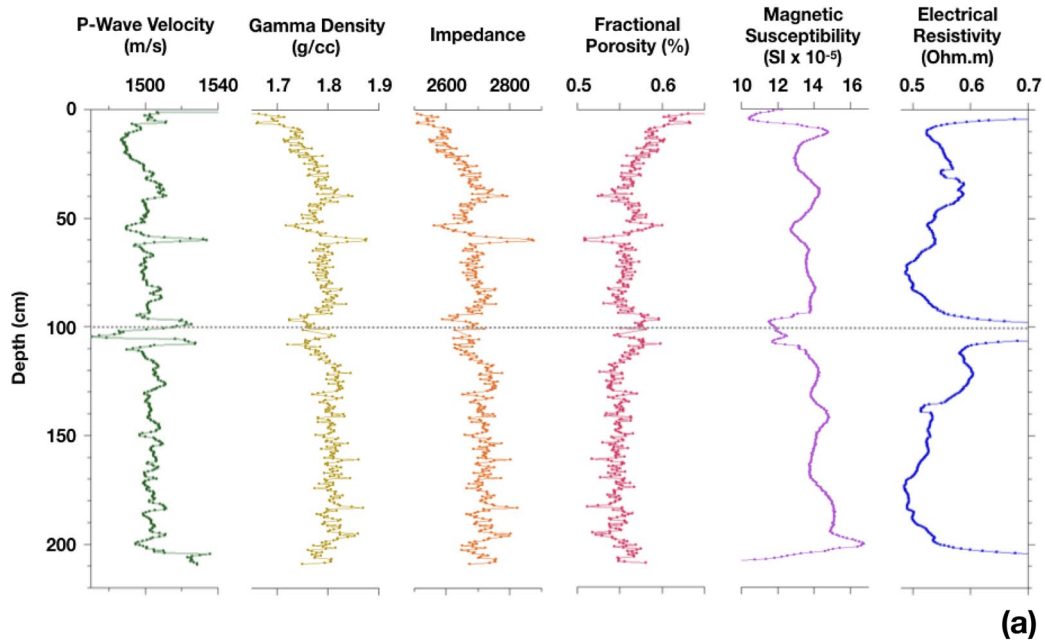
3.3 Chronology and sedimentation rate of LGD-GPC cores

Cores LGD-T32-A-PC and LGD-T43-B-PC were selected to establish chronology based on two AMS ^{14}C dates. The calendar ages of those two core top samples are determined to be modern deposits (Table 2). For the chronology of core LGD-T32-A-PC, the lower part at a depth of 208.5 cm is assigned to 893 ± 164 yr BP. The calculated sedimentation rate is ~0.2 cm/yr (230 cm/kyr). For the almost similar geography of the location at which the identical piston cores were collected, we found that the anomalous sedimentation feature in core LGD-T43-B-PC is twice that of the LGD-T32 core. Core LGD-T43-B-PC recovers a complete sedimentary sequence with a relatively high sedimentation rate (~0.5 cm/yr; 520 cm/kyr) from the past 1316 ± 161 yr BP (Table 2).

3.4 VPCA results from the color reflectance

Due to repeated coring at the same site, the downcore color data spanning different time resolutions were regarded as the same database. Thus, a VPCA was performed by using a factor score matrix composed of 1102 downcore visible core reflectance data from the three LGD-GPC cores. Wavelengths of 400–700 nm were selected for VPCA based on calculations of first-order derivatives. This VPCA method extracts the fewest statistically independent end members for modeling the maximum information that is preserved in the dataset. The results from VPCA revealed that seven significant factors were dominated by a specific combination of wavelengths. We found that seven factors accounted for 87.7% of the total variance of the analyzed color samples (Table 3). The first factor explains 29.8% of the total
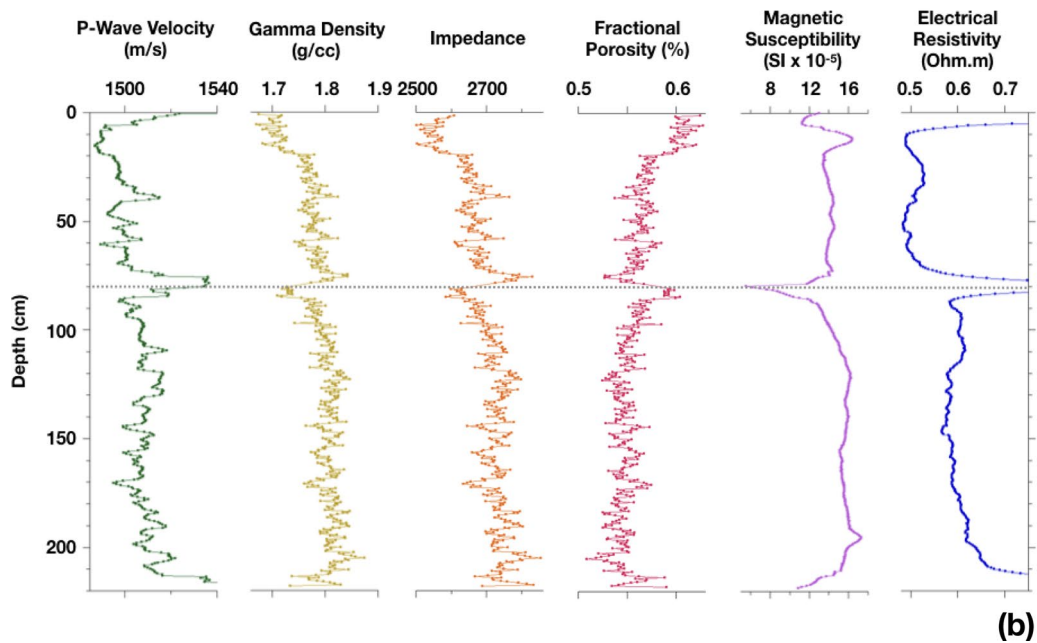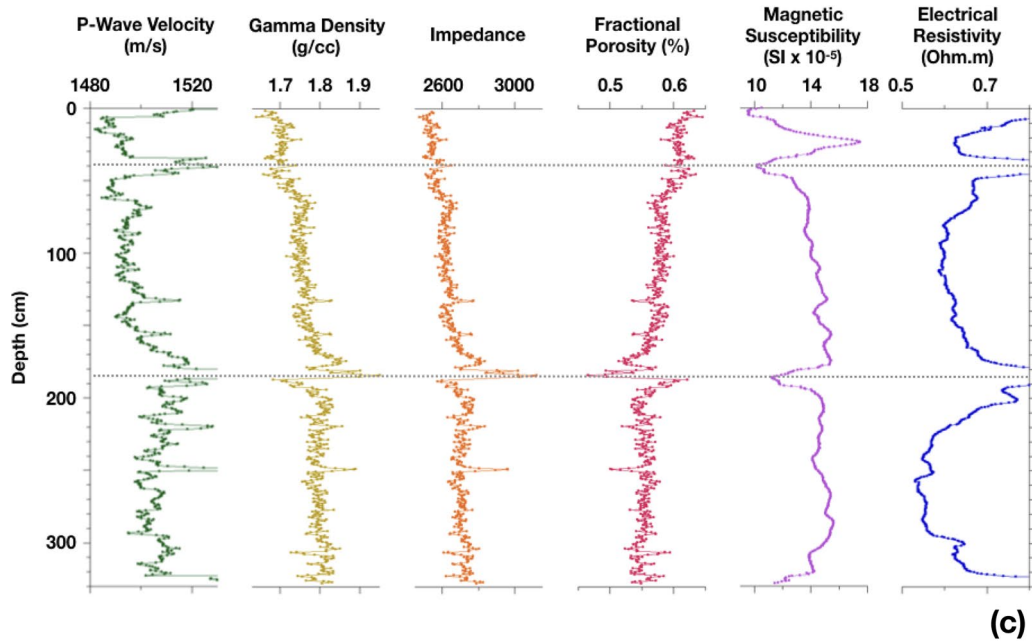
Fig. 4 Physical property measurements derived from MSCL on core **a** LGD-T32-A-PC; **b** LGD-T32-B-PC; **c** LGD-T32-C-GC; and **d** LGD-T43-B-PC. Dashed lines indicate the boundary of core section

Longitude: **120°13.345'E**   Latitude: **22°23.288'N**   Water Depth: **309** m

Sedimentary length: **0 - 328** cm   Core Recovery: **41** %   Site: **LGD-T32-C-GC**

2020.01.14 ~ 01.16

(c)

Longitude: **120°12.531'E**   Latitude: **22°23.493'N**   Water Depth: **355** m

Sedimentary length: **0 - 683** cm   Core Recovery: **85** %   Site: **LGD-T43-B-PC**
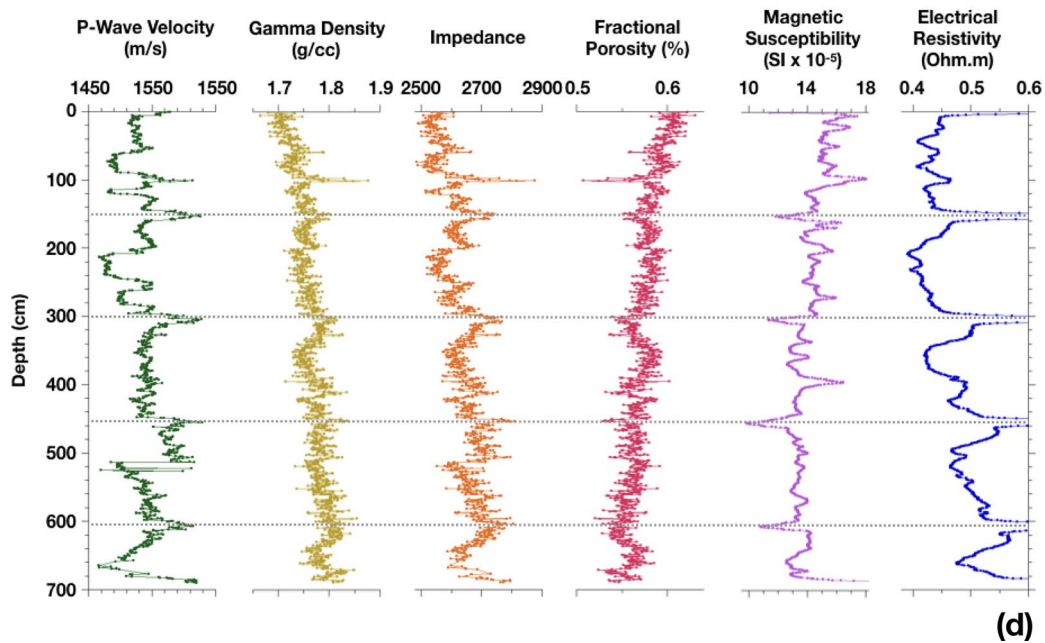
2021.03.30 ~ 04.01

(d)

Fig. 4 continued

Table 3 Varimax factor scores derived from VPCA of those color reflectance database, which is composed of 1102 downcore visible color reflectance data from those three LGD-GPC cores

Wave-length (nm)	Factor 1	Factor 2	Factor 3
400	0.8743	− 0.0054	0.0229
410	0.9153	0.0447	0.0122
420	0.9271	0.0901	− 0.0238
430	0.9057	0.2371	0.0211
440	0.7670	0.4234	0.0947
450	0.7460	0.4888	0.0867
460	0.7449	0.2567	− 0.0192
470	0.6122	0.5337	0.0664
480	0.7510	0.5214	0.0423
490	0.8135	0.4057	0.0193
500	0.5341	0.6796	0.1458
510	0.4666	0.7015	0.1418
520	0.6334	0.6885	0.1161
530	0.7316	0.5590	0.0547
540	0.5850	0.7443	0.1007
550	0.3846	0.8429	0.1575
560	0.3656	0.8738	0.1601
570	0.3734	0.8265	0.1187
580	0.2658	0.8238	0.0459
590	0.1206	0.7972	− 0.0231
600	0.1782	0.5508	0.2014
610	0.1400	0.3076	0.4872
620	0.0239	0.5045	− 0.3163
630	0.0275	0.5100	− 0.4457
640	0.0370	0.0569	0.8790
650	0.1372	0.2890	− 0.2997
660	− 0.0969	0.4138	− 0.5299
670	− 0.0162	0.1984	0.8712
680	0.4354	0.3065	− 0.3394
690	0.3118	0.3199	− 0.0944
700	0.0163	0.1586	0.4721
Variance (%)	29.8	27.3	9.6
Cumulative variance (%)	29.8	57.1	66.8

variance and is entirely dominated at wavelengths of 540–590 nm (Fig. 5a). Factor 2 is characterized by high scores at wavelengths of 400–430 nm, which explains 27.3% of the total variation (Fig. 5b). Although Factors 3 to 7 contribute higher portions of the total variance (< 10%; Factor 4–Factor 7 from 3.2 to 7.4%), we found that the scores of those factors have more noise and hardly identify possible mineral compositions. Thus, interpretations of Factors 3 to 7 are excluded in this study. Most of the contribution of the first two factors (57.1% of the total variance) can be inferred from the major sediment composition and trace further possible sources.

4 Discussion

4.1 Non-destructive measurements for evaluation of giant core quality

4.1.1 Evaluation from non-destructive analyses (MSCL)

We perform non-destructive analyses on giant cores, which have been widely applied to sedimentological studies, gas hydrates investigations and paleoceanographic reconstructions (e.g., WEPAMA/PECTEN cruises, MD 214-EAGER cruise, SONNE 266 cruise; Bassinot et al. 2002; Beaufort et al. 2005; Bohrmann et al. 2023; Huang et al. 2021). In this study, the GRA bulk density and MS provide a relevant platform for stratigraphic correlation in between sediment cores. Observed from those downcore records, we find that fluctuations in the GRA bulk density (associated porosity) are more sensitive in relation to a smooth MS variability (Fig. 3a–d). In general, a long-term increasing trend in the GRA bulk density indicates that this result may be related to compaction, lithified units, and/or dewatering with depth. Results from the digital core images imply that immoderate piston suction during the coring process resulting in the appearance of a distorted sediment structure. This finding further supports that a gradual increase in density is mainly attributed to a strengthening of the sedimentary structures. Rather than lithifying the units themselves, we suggest that the sediment cores experienced a greater pulling force with depth. In this case, the characteristics of the sediment cannot be completely preserved. This would mask some physical properties of sediment (e.g., GRA bulk density) and further yield some possible biases in the stratigraphic correlation.

4.1.2 Evaluation from color reflectance data

In terms of its behavior in downcore factor analysis, we find that variations in Factor 1 loadings have more significant fluctuations than variations in Factor 2 loadings (Fig. 6). The relative pattern in Factor 1 also shows an anti-phase relationship with Factor 2. Distributions of these factor loadings in downcore records indicate that each factor dominates unique sediment compositions or mineral characteristics. The studied sites directly receive fluvial material that is exported from the Kaoping River. The waxing and waning of these two factors may reveal that different sediment sources dominate the downcore variations in this area. Moreover, stratigraphic correlations of these factor loadings are also consistent with the chronology, providing an independent method for age constraints (Fig. 6). Calculated from the sedimentation rates, we observe that the sedimentation rate in core LGD-T43-B-PC is twice as high as that in LGD-T32-A/-B-PC (Table 2). The sedimentary length of core LGD-T43-B-PC is overestimated by more than 200%. This
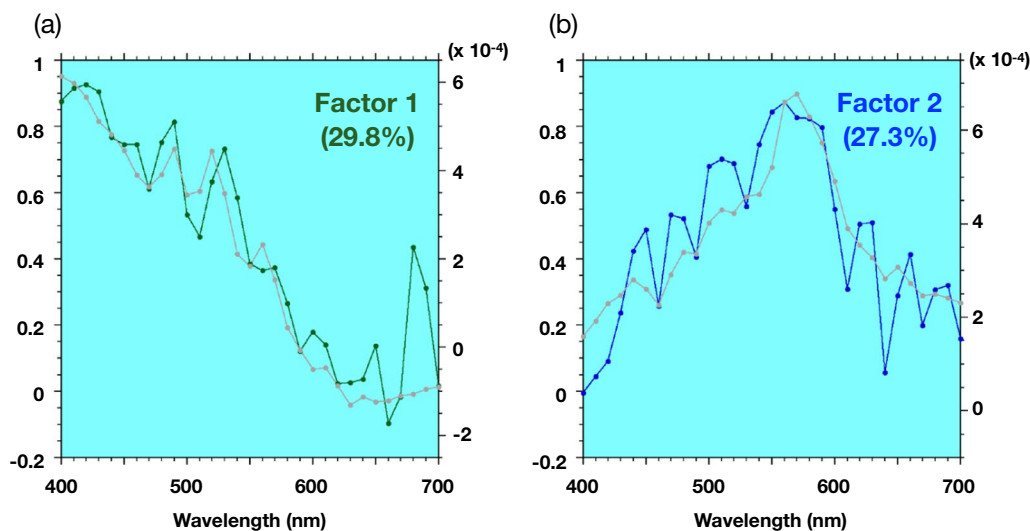
Fig. 5 VARIMAX rotated components (**a** Factor 1, **b** Factor 2) on spectra of the Minolta CM-700d and known mineral standards archived in the laboratory at Kent State University and the USGS Spectral Library plotted as a function of wavelength

finding from color reflectance and AMS ^{14}C dating data further supports that stretching of sediment length is the case for core LGD-T43-B-PC in relation to core LGD-T32-A-PC. We suggest that the modified TORI piston would be a candidate for producing an excessive pulling force inside a tube.

4.1.3 Evaluation from the quantitative index of the CI value
We observe a strong level of distorted sedimentary structures (CI < 4) in most LGD-GPC cores (Fig. 3a) compared with distorted sedimentary structures (10 > CI > 4) in gravity core LGD-T32-C-GC. Evidence from digital surface imaging in core LGD-T32-A-PC, we suggest that shear deformation of sediment against the core barrel would be the prominent factor that govern the core disturbances in LGD-T32 GPC cores (Fig. 3). However, immoderate conditions of the distorted sedimentary structures occur in these marine sediments of core LGD-T43-B-PC (Fig. 3a).

In addition, previous studies have been addressed that stretching effect of the top part of the core (up to ~ 12 m) collected through giant piston coring by the R/V *Marion Dufresne* (Széréméta 2000). This is consistent with what we reconstructed from the western Pacific records during IMAGES III/MD106-IPHIS cruise and WEPAMA cruise (e.g., Wei et al. 2003; Yu et al. 2008; Lin et al. 2013). In this respect, the behavior of the transformation follows an increasing trend in the GRA bulk density, while the pulling force attenuates with depth. However, these transformations and strongly distorted sedimentary structures appear randomly, not with a systemic pattern in sediments. Such a

core disturbance resulted from stretching effect was not commonly observed on other giant piston cores by the R/V *Marion Dufresne*. We suggest that the poor quality of the LGD-GPC cores is due to the inside of the tube undergoing excessive force (i.e., shear deformation).

Moreover, no significant difference existed in the deployment of the LGD-GPC during the cruises, except for a replacement of the modified TORI piston. Observed from distorted sedimentary features in those LGD-GPC cores, we consider that some key mechanisms would dominate the behaviors of those sediments. For the conventional free-fall LGD-GPC, here we exclude the factors of basal flow-in and fall-in that appears on hydraulic piston coring (Jutzeler et al. 2014). Meanwhile, the sediment in the core catcher is composed of homogeneous silty clay to clay. Thus, sediment loss through core catchers is limited. In this study, we suggest that shear deformation of sediment against the core barrel and excessive pulling forcing from a modified TORI piston would be the prominent factors that govern the observed core disturbances in LGD-GPC cores.

In general, perfect sedimentary structures are dependent on a balance between the viscosity of the sediments (friction) and the pulling force from the piston. For identical cores, the characteristics and physical properties of the sediments should have no significant difference. At the revisited site, the friction and the viscosity of those sediment sequences would be similar. Thus, successful work for a piston would be producing a perfect pulling force inside a tube and further acquiring complete sedimentary structures. If the piston indeed works during
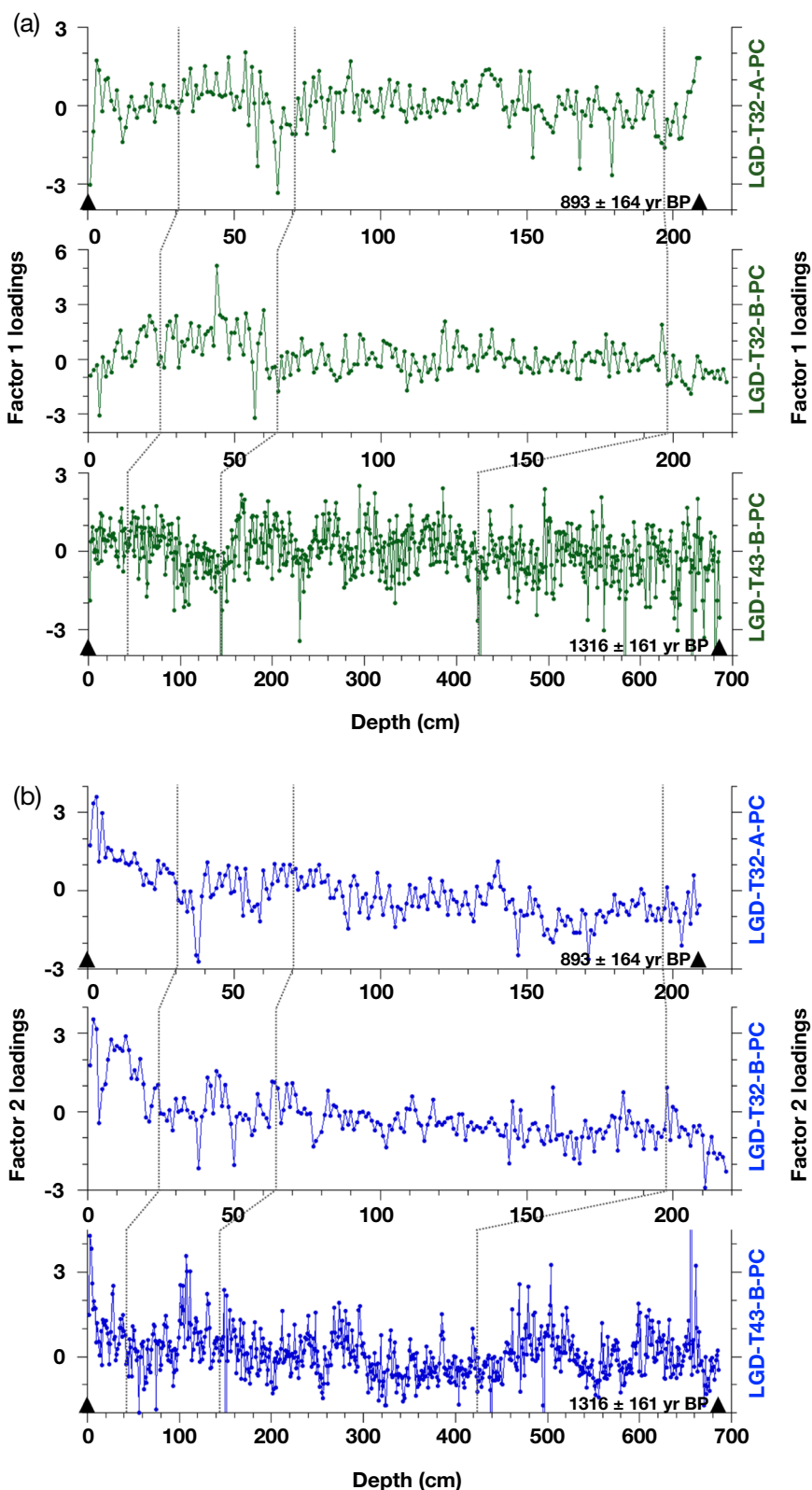
Fig. 6 Factor loadings of the two dominant components (**a** Factor 1, **b** Factor 2) throughout the sediment core. The events were identified and generated by visual alignment of those Factor 1 records (shown by dashed line), and then directly applied to Factor 2. The stratigraphic correlation of these factor loading are also consistent with the chronology among the three LGD-GPC cores. AMS ^{14}C dates (triangles) by planktic foraminifer shell are shown

LGD-GPC, the pulling force overcoming the friction causes distorted sedimentary structures while crossing a tipping point. The severely distorted sedimentary structures and the resulting oversampling are speculated to be due to immoderate piston suction during the coring process. Evidence from digital core imaging and the quantitative method of curvature calculation further supports the mechanism of piston suction. Meanwhile, a slowly lift speed during LGD-GPC coring process may further aggravate core disturbances. Thus, distorted sequence can be found at depths of 100–102 cm, 200–206 cm in LGD-T43-B-PC.

In summary, we suggest that transformation and distorted sedimentary features would potentially be generated by different piston suctions during the coring process, as evidenced by integrated results from non-destructive analyses and quantitative indices. To improve the core quality of LGD-GPC cores and understand plausible mechanisms during the coring process, future research should not only collect enough piston cores but also gather sufficient information on non-destructive measurements. Besides, some parameters for LGD-GPC to improve the core quality included: adjustments of free-fall height of LGD-GPC, penetration speed and lift speed, penetration depth during core operation. In experiments with idealized modeling simulation for the behavior of piston suction, further simulation will be needed to understand its interactions between the pulling force and sediments.

5 Conclusions

Using non-destructive core analyses of MSCL measurements, color reflectance, and digital core imaging from multiple cores offshore SW Taiwan during the LGD-T32 and LGD-T43 cruises, we interpreted the analyzed data in those downcore records as expressions of core quality and drew the following conclusions.

1. Our non-destructive analyses and digital core imaging reveal that strongly sediment deformations occurred in LGD-GPC cores during the LGD-T43 cruise. The immoderate piston suction during the coring process further supports that a gradual increase in density was mainly attributed to a distortion of the sedimentary structures.

2. Color reflectance and AMS ^{14}C dating data further support that oversampling and distorted sedimentary features appear in core LGD-T43-B-PC in relation to core LGD-T32-A-PC. We suggest that the TORI-revised piston would be a candidate for producing excessive pulling force inside a tube.

3. We suggest that shear deformation of sediment against the core barrel and excessive pulling forcing from a modified TORI piston would be the prominent factors that govern the observed core disturbances in LGD-GPC cores.

4. For distorted sedimentary sequences, we suggest that an integrated method of CI and color reflectance measurements is another technique for evaluating the stratigraphic correlation and core quality than only using physical property analysis from the MSCL.

Supplementary Information

The online version contains supplementary material available at https://doi.org/10.1007/s44195-023-00048-0.

Additional file 1: Table S1. The depths, heights of the curvature and the calculation of CI values from core LGD-T43-B-PC are listed. **Fig. S1.** Digital images of core LGD-T43-B-PC. **Fig. S2.** X-ray images of core LGD-T43-B-PC.

References
Bassinot F, Baltzer A, Chen M-T, DeDeckker P, Khuhnt W, Levitan M, Nurnberg D, Oba T, Prentice M, Sanrthein M, Situmorang M, Tiedemann R, Holbourn A, Kiefer T, Pflaumann U, Rothe S (2002) Scientific Report of the WEPAMA Cruise, MD122/IMAGES VII. Institut Francais pour la Recherche et la Technologie Polaires, France, 453 pp

Beaufort L, Chen M-T, Droxler A, shipboard scientific party (2005) MD148/PECTEN - IMAGES XIII Cruise Report. Les rapports de campagnes à la mer, Institute Polaire Francais Paul Emile Victor, Brest, France, 58 pp

Bé AWH (1967) Foraminifera, families: *Globigerinidae* and *Globorotaliidae*. In: Fraser JH (ed), Fiches d'Indentification du Zooplancton, Cons. Int. Explor. Mer, Charlottenlund, Denmark, Sheet 108

Bohrmann G, Berndt C, Lin S, Tu T-H, Lin A, Hsu H-H, Lai M-C, Chi W-C, Deusner C, Elger J, Wallmann K, Freudenthal T, Mau S, Pape T, Tseng Y-T, Yu P-S, Fan L-F, Chen J-N, Chen S-C, Chen T-T, Wei K-Y, SONNE SO266 shipboard scientific party (2023) Geological controls on the distribution of gas hydrates in the shallow parts of the gas hydrate stability zone—constraints from seafloor drilling off Taiwan. Mar Petrol Geol. https://doi.org/10.1016/j.marpetgeo.2023.106253

Chen M-T, Beaufort L, The Shipboard Scientific Party of the IMAGES III/MD106-IPHIS Cruise (Leg II) (1998) Exploring Quaternary variability of the East Asian monsoon, Kuroshio Current, and the Western Pacific warm pool systems: High-resolution investigations of paleoceanography from the IMAGES III/MD106-IPHIS cruise. Terr Atmos Ocean Sci 9:129–142

Chen M-T, Chang Y-P, Yu P-S, Shiau L-J (2010) Marine records of east Asian monsoon variability over the past 5 Myr. Monsoon evolution and tectonics-climate linkage in Asia. J Geol Soc Spe Publ Lond 342:5–15. https://doi.org/10.1144/SP342.2

Huang Y-S, Hsu S-K, Su C-C, Lin T-S, Yu P-S, Babonneau N, Ratzov G, Lallemand S, Lin S-S, Huang P-C, Lin J-Y, Wei K-Y, Chang Y-P, Yu N-T, Tsai C-H, Chen S-C (2021) Shallow gas hydrates off southwest Taiwan and their mechanisms. Mar Geophys Res. https://doi.org/10.1007/s11001-021-09429-x

Huh C-A, Lin H-L, Lin S-W, Huang Y-W (2009) Modern accumulation rates and a budget of sediment off the Gaoping (Kaoping) River, SW Taiwan: a tidal and flood dominated depositional environment around a submarine canyon. J Mar Syst 76:405–416

Imbrie J, Kipp KG (1971) A new micopaleontological method for quantitative paleoclimatology: application to a late Pleistocene Caribbean core. In: Turekian KK (ed) The late Cenozoic glacial ages. Yale Univ Press, New Haven, pp 71–181

IPCC (2021) Climate change 2021: the physical science basis. Contribution of Working Group I to the Sixth Assessment Report of the Intergovernmental Panel on Climate Change. In: Masson-Delmotte V, Zhai P, Pirani A, Connors SL, Péan C, Berger S, Caud N, Chen Y, Goldfarb L, Gomis MI, Huang M, Leitzell K, Lonnoy E, Matthews JBR, Maycock TK, Waterfield T, Yelekçi O, Yu R, Zhou B (Eds.), Cambridge Univ. Press, Cambridge, United Kingdom and New York, NY, USA, 2391 pp. doi:https://doi.org/10.1017/9781009157896

Jutzeler M, White JDL, Talling PJ, McCanta M, Morgan S, Le Friant A, Ishizuka O (2014) Coring disturbances in IODP piston cores with implications for offshore record of volcanic events and the Missoula megafloods. Geochem Geophys Geosyst 15:3572–3590. https://doi.org/10.1002/2014GC005447

Kipp NG, Brown University (1976) New transfer function for estimating past sea-surface conditions from sea-bed distribution of planktonic foraminiferal assemblages in the North Atlantic. Memoir Geol Soc Am 145:3–41

Lin D-C, Chen M-T, Yamamoto M, Yokoyama Y (2013) Precisely dated AMS 14C marine cores reveal the complexity of millennial-scale Asian monsoon variability in the northern South China Sea (MD972146, MD972148). J Asian Earth Sci 69:93–101

Pan H-J, Yu P-S, Chen M-T (2014) A marine sediment component interpretation based on diffuse reflectance spectrophotometry from northern South China Sea sediment core MD972148. Quat Int 333:20–25

Pan H-J, Yu P-S, Chen M-T (2015) Testing the uncertainty of diffuse reflectance spectroscopy methods for estimating marine sediment components by full-resolution spectrophotometry and principle component analyses. J Asian Earth Sci 114(3):526–533

Parker FL (1962) Planktonic foraminiferal species in Pacific sediments. Micropaleontol 8:219–254

Patrice W, Jean-Francois B, Gilbert D, Loic D, Nabil S (2012) Improving in piston coring quality with acceleration and pressure measurements and new insights on quality of the recovery. 8th International Marine Technicians Symposium, INMARTECH 2012, Texel, The Netherlands

Skinner LC, McCave IN (2003) Analysis and modelling of gravity and piston coring based on soil mechanics. Mar Geol 199:181–204

Stuiver M, Reimer PJ, Reimer RW (2005) Calib radiocarbon calibration program CALIB 8.2 [WWW program and documentation] (http://calib.qub.ac.uk/)

Stuiver M, Reimer PJ (1993) Extended ^{14}C data base and revised CALIB 3.0 ^{14}C age calibration program.Radiocarbon 35:215–230

Széréméta N, Bassinot FC, Kissel C, Bault Y, Guibert K, Dubois K, Laj C, Pagel M (2000) Stretching of sedimentary series collected through piston coring: evidences, implications and corrections (abstract). EOS Trans AGU 81(48):F708

Tommasi P, Avalle A, Budillon F, Romeo R, Caburlotto A, Conforti A, Di Martino G, Pagliaroli A, Magagnoli M, Urgeles R, Llopart J, Camerlenghi A (2019) Evaluation of disturbance induced on soft offshore sediments by two types of gravity piston coring techniques. Mar Geol 417:106005. https://doi.org/10.1016/j.margeo.2019.106005

Wei K-Y, Chiu TC, Chen Y-G (2003) Toward establishing a maritime proxy record of the East Asian summer monsoons for the late Quaternary. Mar Geol 201:67–79

Yu P-S, Mii H-S, Murayama M, Chen M-T (2008) Late Quaternary planktic foraminifer fauna and monsoon upwelling records from the western South China Sea, near Vietnam Margin (IMAGES MD012394). Terr Atmos Ocean Sci 19(4):347–362

Yu P-S, Kienast M, Chen M-T, Cacho I, Flores JA (2017) Surface hydrographic and water mass variability in the eastern equatorial Pacific during interglacial-like Marine Isotope Stage 14. Quat Int 436(A):45–56

Publisher's Note